



Antiproliferative Activity of Cationic and Neutral thiosemicarbazone Copper(II) Complexes

Journal:	<i>RSC Advances</i>
Manuscript ID	RA-ART-12-2015-026071.R2
Article Type:	Paper
Date Submitted by the Author:	11-Feb-2016
Complete List of Authors:	Mohamed Kasim, Mohamed Subarkhan; Bharathidasan University, School of Chemistry Ramasamy, Raj; Bharathidasan University, School of Chemistry Narayana Prabhu, Rupesh; University of Hyderabad, School of Chemistry Rengan, Ramesh; Bharathidasan University, School of Chemistry;
Subject area & keyword:	Bioinorganic chemistry < Chemical biology & medicinal



Journal Name

ARTICLE

Antiproliferative Activity of Cationic and Neutral thiosemicarbazone Copper(II) Complexes

Received 00th January 20xx,
Accepted 00th January 20xx

DOI: 10.1039/x0xx00000x

www.rsc.org/

M. Mohamed Subarkhan,^a Rupesh N. Prabhu,^b R. Raj Kumar^a and R. Ramesh,^{a,*}

The copper(II) complexes, [Cu(tscpy)(MeOH)](Cl) (**1**), [CuCl(mtscpy)] (**2**) and [CuCl(ptscpy)] (**3**) (where, Htscpy = pyridoxal thiosemicarbazone, Hmtscpy = pyridoxal N⁴-methyl thiosemicarbazone and Hptscpy = pyridoxal N⁴-phenylthiosemicarbazone) have been isolated and characterized by the aid of various analytical and spectral methods. The molecular structure of the cationic complex **1** and the neutral complex **3** were characterized by single crystal X-ray diffraction studies which revealed that the thiosemicarbazone ligands coordinated to copper(II) centre as monoanionic tridentate (ONS⁻) forming five and six membered rings. The interaction of the new complexes with DNA has been explored using spectral and viscosity studies, indicating the complexes bind to DNA via partial intercalation. A predominantly hydrolytic cleavage of supercoiled pUC19 plasmid DNA was confirmed through experiment performed in the presence of T4 ligase. Further, the interactions of the complexes with serum albumin (BSA) were also investigated using fluorescence spectroscopic methods. The efficiency of the complexes in arresting the growth of human cervical cancer cells (HeLa), human breast cancer cell line (MCF-7) and human liver carcinoma cells (Hep G2) has also been studied along with the cell viability assay against the noncancerous NIH 3T3 mouse embryonic fibroblasts cell lines under in vitro conditions. The cationic complex **1** has higher cytotoxic activity than the other two neutral complexes and cisplatin. AO-EB/DAPI staining assays, Annexin V-FITC and FACS analyses indicated that the complex **1** induces cell death only by apoptosis.

Introduction

Cancer is one of the diseases involving abnormal cell growth with the potential to invade or spread to other parts of the body. Platinum-based chemotherapy drugs such as cisplatin, oxaliplatin, nedaplatin, lobaplatin and carboplatin are some of the chemotherapeutic agents in clinical use.¹⁻³ The platinum-based cancer drugs destroy tumor cells by binding to DNA strands and prevent the DNA replication. In addition, these drugs have several disadvantages such as limited solubility, severely dose-limiting side effects such as neurotoxicity, nephrotoxicity, ototoxicity, nausea and intrinsic or acquired resistance in some cancer types.⁴⁻⁶ These problems have stirred a wide search and prompted chemists to develop alternative methods, based on various metals, with improved pharmacological interest and aimed at different targets.⁷⁻¹⁰

Copper(II) complexes has been established that the properties of copper-coordinated compounds are largely determined by the nature of ligands, substituents present on the ligands and

donor atoms bound to the metal ion.^{11,12} Recently, several copper(II) complexes have been reported as potential anticancer and chemotherapeutic agents and many copper complexes have been established to be active both in vitro and in vivo.^{13,14} Many copper(II) complexes possessing multidentate ligands have found to strongly bind to DNA, efficiently cleave DNA and exhibit prominent cytotoxicity by inducing apoptosis.¹⁵⁻²⁰ At the same time, proteins have also attracted enormous research interest as a prime molecular target.²¹ Bovine serum albumin (BSA) is soluble protein that has the ability to transport a multitude of endogenous and exogenous ligands such as fatty acids, amino acids, steroids, metal ions and drugs in blood stream. It is used to study interaction between protein-drug complex in the circulatory system because it has same structural similarity with human serum albumin (HSA). It is essential to search drug-protein interactions as most of the drugs bound to BSA are usually transported as a protein complex.²² Therefore, the study of the binding properties of metal complexes with protein is of great significance for the design of new drugs and their applications.²³

Additionally, thiosemicarbazones are a class of Schiff bases which are considered to be one of the most important scaffolds that have been explored because of their broad spectrum of biological activities.²⁴ Brockman et. al. first reported that 2-formylpyridine thiosemicarbazone possesses antileukemic activity in mice.²⁵ Following this several copper thiosemicarbazone complexes being investigated as potential

^aSchool of Chemistry, Bharathidasan University, Tiruchirappalli 620 024, Tamil Nadu, India.

^bSchool of Chemistry, University of Hyderabad, Hyderabad 500 046, Telangana, India.

† Electronic supplementary information (ESI) available: CCDC numbers 1025349 and 1056113 for the copper(II) complexes **1** and **3** respectively. Selected bond length and bond angles are provided.

See DOI: 10.1039/x0xx00000x

anticancer therapeutics, especially for prostate, stomach, cervical, ovarian, breast and lung cancer, where elevated levels of intracellular copper have been demonstrated.^{26,27} Cytotoxicity of copper(II) complexes with thiosemicarbazone ligands containing a pyrazolone moiety have been studied on the HL60, REH, C6, L929 and B16 cell lines.²⁸ Donnelly et. al. have reported the cell permeability and intracellular distribution of pyrene-appended bis(thiosemicarbazonato) copper(II) complexes using confocal fluorescence microscopy.²⁹ While many copper(II) thiosemicarbazone complexes exhibit good biological activities, their water solubility is still unsatisfactory, which may restrict their application.

In this report, the synthesis and characterisation of three new water soluble copper(II) complexes bearing pyridoxal thiosemicarbazone ligand have been described. The interaction of these complexes with calf-thymus DNA (CT-DNA) utilizing UV-Vis absorption titration, competitive DNA binding fluorescence experiments, circular dichroism study and viscosity measurements were performed. Further, their cleavage activity with supercoiled pUC19 DNA along with T4 ligase was probed using gel electrophoresis. The protein binding property of these complexes was also studied by fluorescence spectroscopic techniques. Further, the in vitro anticancer activity of these complexes and cell death were also investigated.

Experimental section

All reagents and solvents were purchased commercially and were used as received. Copper(II) chloride dihydrate, substituted thiosemicarbazides, ethidium bromide (EB), calf thymus (CT) DNA (highly polymerized, stored at $-20\text{ }^{\circ}\text{C}$) (Sigma-Aldrich, USA), supercoiled pUC19 DNA, agarose and bovine serum albumin (BSA) (Genei) were used as received. Solvents were purified and dried according to standard procedures.³⁰ The human cervical cancer cell line (HeLa), human breast cancer cell line (MCF-7), human liver carcinoma cell line (Hep G2) and mouse embryonic fibroblast cell line (NIH 3T3) were obtained from the National Centre for Cell Science (NCCS) Pune, India. $[\text{CuCl}_2(\text{DMSO})_2]$ was prepared by the reaction of copper(II) chloride and DMSO according to previously reported method.³¹ The Schiff bases were prepared as their hydrochloride salts in $\sim 85\%$ yield from pyridoxal hydrochloride with different thiosemicarbazides (thiosemicarbazide for HtscpyHCl, methyl thiosemicarbazide for HmtscpyHCl, phenyl thiosemicarbazide for HptscpyHCl) similar to that reported earlier.³² All other chemicals and reagents used for the biological studies were of high quality in biological grade. Doubly distilled water was used to prepare buffers and biological solutions. For the biological studies, concentrated stock solutions of metal complexes were prepared by dissolving them in a 2% DMF – 5 mM Tris-HCl/50 mM NaCl buffer solution (0.5 mL of DMF in 5 mL of buffer) at pH 7.2 and diluting them suitably with the corresponding buffer to required concentrations for all the experiments.

Melting points were recorded in the Boetius micro heating table and are uncorrected. Elemental (C, H and N) analyses were performed on a Vario EL III CHNS elemental analyzer. Magnetic susceptibility measurements were performed with the help of a Sherwood scientific balance. A Systronics digital conductivity meter 304 was used to measure the molar conductivities of the complexes. IR spectra of the samples were recorded as KBr pellets on a Perkin-Elmer 597 spectrophotometer instrument in the frequency range of 400–4000 cm^{-1} . UV-Vis spectroscopy was recorded on a Varian Cary 300 Bio UV-Vis spectrophotometer using cuvettes of 1 cm path length. The X-band EPR spectra of the complexes in dichloromethane solution at 77 K were recorded on Jeol JES-FA200 EPR spectrometer. A Micro mass Quattro II triple quadrupole mass spectrometer was employed for Electrospray ionization mass spectrometry (ESI-MS), Emission intensity measurements were carried out using a Jasco FP-6200 spectrofluorometer. Induced circular dichroism spectra were recorded on JASCO J-810 spectropolarimeter with PMT detector in DMSO-buffer solution. Circular dichroism experiments were carried out using a quartz cell of 1 cm path length. Each CD spectrum was collected after averaging over at least 4 accumulations using a scan speed of 100 nm/min. The viscosity measurements were carried out on a Schott Gerate AVS 310 viscometer thermostat at $28\text{ }^{\circ}\text{C}$ in a constant temperature bath.

Synthesis of copper(II) complexes

Synthesis $[\text{Cu}(\text{tscpy})(\text{MeOH})]\text{Cl}$ (1)

A solution containing $[\text{CuCl}_2(\text{DMSO})_2]$ (145 mg, 0.5 mmol) in DMF (20 mL) was added to a warm methanolic solution (10 mL) of Htscpy-HCl (134 mg, 0.5 mmol) and refluxed for 30 min. Green single crystals suitable for X-ray studies were obtained on slow evaporation of the reaction mixture over a period of 10–15 days. Yield: 1.09 g (72%). Melting point: $274\text{--}278\text{ }^{\circ}\text{C}$. Elemental analysis calculated for (%) $\text{C}_{10}\text{H}_{15}\text{ClCuN}_4\text{O}_3\text{S}$: C, 32.43; H, 4.08; N, 15.13. Found (%) C, 32.32; H, 3.98; N, 15.01. Selected IR data: ν_{max} (cm^{-1}): 1595 (s) $\nu(\text{C}=\text{N})$; 828 (m) $\nu(\text{C}=\text{S})$. UV-visible (solvent: Tris-HCl buffer; λ_{max} : nm, ϵ_{max} : $\text{M}^{-1}\text{ cm}^{-1}$): 330 (11760), 413 (13160). μ_{eff} (300 K): 1.79 μB . EPR (77 K, CH_2Cl_2): $g_{\parallel} = 2.409$, $g_{\perp} = 1.897$. Molar conductance, M (1×10^{-3} M, DMSO): 89 $\text{S cm}^2\text{ mole}^{-1}$. ESI-MS: $\{[\text{Cu}(\text{tscpy})(\text{MeOH})(\text{Cl})+\text{H}]^+\}$ displays a peak at m/z 369.76 (calcd m/z 370.02).

Synthesis of $[\text{CuCl}(\text{mtscpy})]$ (2)

The complex **2** was prepared by adopting the procedure used for obtaining **1** by using Hmtscpy-HCl (129 mg, 0.5 mmol) instead of Htscpy-HCl. Green colored solid was formed by the slow evaporation of the reaction mixture. Yield: 1.04 g 68%. Melting point: $264\text{--}270\text{ }^{\circ}\text{C}$. Elemental analysis calculated for (%) $\text{C}_{11}\text{H}_{16}\text{ClCuN}_4\text{O}_2\text{S}$: C, 35.97; H, 4.39; N, 15.25. Found (%) C, 36.07; H, 4.30; N, 15.17. Selected IR data: ν_{max} (cm^{-1}): 1591 (s) $\nu(\text{C}=\text{N})$; 839 (m) $\nu(\text{C}=\text{S})$. UV-visible (solvent: Tris-HCl buffer; λ_{max} : nm, ϵ_{max} : $\text{M}^{-1}\text{ cm}^{-1}$): 331 (11760), 413 (13160). μ_{eff} (300 K): 1.80 μB . EPR (77 K, CH_2Cl_2): $g_{\parallel} = 2.373$, $g_{\perp} = 1.736$. Molar conductance, M (1×10^{-3} M, DMSO): 9 $\text{S cm}^2\text{ mole}^{-1}$. ESI-MS:

$\{[\text{CuCl}(\text{mtsncpy})+\text{H}]^+\}$ displays a peak at m/z 352.83 (calcd m/z 352.76).

Synthesis of $[\text{CuCl}(\text{ptsncpy})]$ (**3**)

The complex **3** was prepared by using the procedure employed for obtaining **1** by using Hptsncpy·HCl (165 mg, 0.5 mmol) instead of Htsncpy·HCl. Green single crystals suitable for X-ray studies were obtained on slow evaporation of the reaction mixture over a period of 10–15 days. Yield: 1.12 g (74%). Melting point: 230–235 °C. Elemental analysis calculated for (%) $\text{C}_{16}\text{H}_{18}\text{ClCuN}_4\text{O}_2\text{S}$: C, 44.75; H, 4.23; N, 13.05. Found (%) C, 44.84; H, 4.18; N, 13.00. Selected IR data: ν_{max} (cm^{-1}): 1588 (s) $\nu(\text{C}=\text{N})$; 847 (m) $\nu(\text{C}=\text{S})$. UV-visible (solvent: Tris-HCl buffer; λ_{max} : nm, ϵ_{max} : $\text{M}^{-1}\text{cm}^{-1}$): 328 (11760), 415 (13160). μ_{eff} (300 K): 1.82 μB . EPR (77 K, CH_2Cl_2): $g_{\parallel} = 2.381$, $g_{\perp} = 1.767$. Molar conductance, M (1×10^{-3} M, DMSO): 12 $\text{S cm}^2 \text{mole}^{-1}$. ESI-MS: $\{[\text{CuCl}(\text{mtsncpy})+\text{H}]^+\}$ displays a peak at m/z 413.72 (calcd m/z 414.07).

Single crystal X-ray diffraction studies

Single crystals of **1** and **3** were obtained by slow evaporation of the reaction mixture at room temperature. **1** crystallizes without any solvent molecule, whereas **3** crystallizes as the solvate (as 3-DMF·H₂O). Determination of the unit cell parameters and the intensity data collections at 298 K were carried out using monochromated Mo K_{α} radiation ($\lambda = 0.71073$ Å) on Bruker–Nonius SMART APEX CCD single crystal X-ray diffractometer. The SMART and the SAINT-Plus packages³³ were used for data acquisition and data extraction, respectively and SADABS program³⁴ was used for absorption correction. The structures were solved by SHELXS–97 and refined by full-matrix least squares procedures using SHELXL–97 programs,³⁵ respectively. Both programs were accessed through the WinGX package.³⁶ The non-hydrogen atoms with full site occupancies were refined anisotropically. The hydrogen atoms in both structures were included in the structure factor calculations at idealized positions by using a riding model. The Platon³⁷ and the Mercury³⁸ packages were used for molecular graphics. The relevant data concerning data collection and details of structure refinement for the two structures are summarized in Table 1.

Stability studies

The stabilities of complexes **1–3** were checked by recording the UV-visible spectrum of them by dissolving in a minimum amount of DMSO (1×10^{-3} M), and then diluted with PBS buffer. The hydrolysis profiles of these complexes were recorded by monitoring the electronic spectra for the resulting mixture over 24 h.

Table 1. Selected crystal data and structure refinement summary of **1** and **3**·DMF·H₂O

Complex	1	3-DMF·H ₂ O
CCDC Number	1025349	1056113
Chemical formula	C10H15ClCuN4O3S	C18H24ClCuN5O4S
Formula weight	370.31	505.47
Crystal system	Triclinic	Monoclinic
Space group	P $\bar{1}$	C2/c
a (Å)	7.685(4)	24.526(13)
b (Å)	9.476(5)	10.497(6)
c (Å)	10.132(5)	16.882(9)
α (°)	99.684(8)	90.00
β (°)	102.043(9)	95.056(8)
γ (°)	94.185(8)	90.00
Volume (Å ³)	706.8(6)	4329(4)
Z	2	8
ρ (g cm ⁻³)	1.740	1.551
μ (mm ⁻¹)	1.893	1.264
Reflections collected	6137	21040
R1, wR2 [$\geq 2\sigma(I)$]	0.0465, 0.1288	0.0857, 0.1734
Goodness-of-fit on F ²	1.023	1.047

DNA binding experiments

Concentrated DNA stock solution was prepared by dissolving them in a 2% DMF – 5 mM Tris–HCl/50 mM NaCl buffer solution (0.5 mL of DMF in 5 mL of buffer) at pH 7.2 and diluting them suitably with the corresponding buffer to required concentrations for all the experiments. The stock solution of CT DNA gave a ratio of UV absorbance at 260 and 280 nm (A_{260}/A_{280}) of 1.89, indicating that the DNA was sufficiently free of protein contamination. The DNA concentration per nucleotide was determined by UV absorbance measurements at 260 nm after 1:20 dilution using the extinction coefficient 260 as $6600 \text{ M}^{-1} \text{ cm}^{-1}$.³⁹ Stock solutions were stored at 4 °C and used within 4 days. Absorption titration experiments were performed by maintaining a constant concentration of the complexes (25 μM), but varying the DNA concentration (0–50 μM) in buffer. This was achieved by dissolving an appropriate amount of the complex and DNA stock solutions while maintaining the total volume constant (1 mL). This results in a series of solutions with varying concentrations of DNA but with a constant concentration of the complex. The absorbance was recorded after successive additions of CT-DNA with an equilibration time of 3 min, allowing the complexes to bind to CT-DNA.

The apparent DNA binding constants (K_{app}) of the copper(II) complexes was determined using ethidium bromide (EB) displacement assay. The emission intensity of EB was used as a spectral probe, as EB shows reduced emission intensity in buffer solution due to solvent quenching whereas an enhancement of the emission intensity is observed when EB intercalatively binds to CT-DNA. DNA in Tris–HCl buffer was pretreated with EB in the 1:1 ratio for 15 minutes. The changes in the fluorescence intensity of EB bound to DNA at 607 nm (546 nm excitation) upon the addition of the increasing amounts of copper(II) complexes was recorded. The excitation

and emission slit widths as well as scan rates were maintained constant for all of the experiments. Circular dichroic spectra were obtained using 1 cm path length quartz cell at room temperature. Circular dichroic experiments were carried out by keeping the concentration of CT-DNA constant but varying the concentration of the copper(II) complexes and by monitoring the changes in the positive peak and negative peak of CT-DNA. The viscosity measurements were carried out at 28 °C. The flow time was measured with a stopwatch and each sample was tested, three times to get an average calculated time DNA samples approximately 200 bp in average length were prepared by sonicating in order to minimize complexities arising from DNA flexibility. Titrations were performed for the complexes (3 μM), and each complex was introduced into the CT-DNA solution (50 μM) present in the viscometer. The data were presented as $(\eta/\eta_0)^{1/3}$ versus the ratio of the concentration of the complex to CT-DNA, where η is the viscosity of CT-DNA in the presence of the complex, and η_0 is the viscosity of CT-DNA alone. The viscosity values were calculated from the observed flow time (t) of CT-DNA containing solutions corrected from the flow time of buffer alone (t_0), $\eta = (t - t_0)/t_0$.

DNA cleavage experiments

Plasmid pUC19 DNA was stored at -20 °C, and the concentration of DNA in base pairs was determined by UV absorbance at 260 nm after appropriate dilutions taking ϵ_{260} as $13100 \text{ M}^{-1} \text{ cm}^{-1}$.⁴⁰ The interaction of complexes with supercoiled pUC19 DNA was monitored using agarose gel electrophoresis. The ability of the copper(II) complex to cleave DNA was assayed with the aid of gel electrophoresis on pUC19 DNA as the substrate in a medium of Tris-HCl buffer (5 mM) with 50 mM NaCl (pH = 7.2) was treated with the complexes at different concentration (5-30 μM) by dilution with the Tris-HCl buffer to a total volume of 20 μL. The samples were then incubated for 1 h at 37 °C and analysed for the cleaved products using gel electrophoresis. A loading buffer containing 25% bromophenol blue, 0.25% xylene cyanol, 30% glycerol was added and electrophoresis performed at 50 V for 2 h in Tris-Acetate-EDTA (TAE) buffer using 1% agarose gel containing $1.0 \mu\text{g mL}^{-1}$ EB. The gels were viewed in a Gel doc system and photographed using a CCD camera (Alpha Innotech Corporation). Densitometric calculations were made using the Alpha Ease FC Stand Alone software. The cleavage efficiency were determined by the ability of the complex to convert the supercoiled SC DNA (Form-I) to nicked circular NC (Form-II).

T4 DNA Ligase Experiment

Ligation enzymatic assay was performed using T4 DNA ligase to determine whether the cleaved products consistent with hydrolytic cleavage of DNA. The cleavage product was purified by DNA gel extraction kit and incubated for 12 h at 16 °C with 1.5 mL of $10\times$ ligation buffer, 1 μL of T4 ligase (4 units) and 2.5 μL of 1 μM ATP. Afterwards, the ligation products were stained with EtBr, electrophoresed and imaged.

Protein binding studies

Protein-binding studies using bovine serum albumin (BSA) was investigated by fluorescence quenching experiments. The excitation wavelength of BSA at 280 nm and the emission at 349 nm were monitored for the protein binding studies. The excitation and emission slit widths and scan rates were maintained constant for all of the experiments. Samples were carefully degassed using pure nitrogen gas for 15 min. Quartz cells (4 x 1 x 1 cm) with high vacuum Teflon stopcocks were used for degassing. The excitation and emission slit widths as well as scan rates were maintained constant for all of the experiments. A stock solution of BSA was prepared in 50 mM phosphate buffer (pH = 7.2) and stored in the dark at 4 °C for further use. A concentrated stock solution of the complexes was prepared as mentioned for the DNA binding experiments, except that the phosphate buffer was used instead of a Tris-HCl buffer for all of the experiments. Titrations were manually done by a micropipette for the addition of the copper(II) complexes.

Cytotoxicity assay

The IC_{50} values, which are the concentrations of the tested compounds that inhibit 50% of cell growth, were determined using a 3-(4,5-dimethyl thiazol-2-yl)-2,5-diphenyl tetrazolium bromide (MTT) assay. Cells were plated in their growth medium at a density of 5000 cells per well in 96 flat bottomed well plates. After 24 h plating, the copper complexes were added at various concentrations for 24 h to study the dose dependent cytotoxic effect. To each well, 20 μL of 5 mg mL^{-1} MTT in phosphate-buffer (PBS) was added. The plates were wrapped with aluminium foil and incubated for 4 h at 37 °C. The purple formazan product was dissolved by addition of 100 μL of 100% DMSO to each well. The quantity of formazan formed gave a measure of the number of viable cells. HeLa, MCF-7, Hep G2 and NIH 3T3 were used for the MTT assay. The absorbance was monitored at 570 nm (measurement) and 630 nm (reference) using a 96 well plate reader (Bio-Rad, Hercules, CA, USA). Data were collected for four replicates each and used to calculate the respective means. The percentage of inhibition was calculated, from this data, using the formula: Percentage inhibition = $100 \times \{ \text{Mean OD of untreated cells (control)} - \text{Mean OD of treated cells} \} / \{ \text{Mean OD of untreated cells (control)} \}$. The IC_{50} value was determined as the complex concentration that is required to reduce the absorbance to half that of the control.

Acridine orange and ethidium bromide staining experiment

The changes in chromatin organization in MCF-7 cells after treatment with complex **1** by dual staining method using acridine orange (AO) and ethidium bromide (EB). Briefly, about 5×10^5 cells were allowed to adhere overnight on a coverslip placed in each well of a 12-well plate. The cells were allowed to recover for 1 h, washed thrice with DPBS, stained with an AO and EB mixture (1:1, 10 μM) for 15 min, and observed with a confocal microscope LSM 710 (Carl Zeiss, Germany).

DAPI staining method

DAPI (4',6'-diamidino-2-phenylindole) staining was done using the method described earlier with slight modifications. 5×10^5 MCF-7 cells were treated with complex **1** for 24 h in a 6-well culture plate and were fixed with 4% paraformaldehyde followed by permeabilization with 0.1% Triton X-100. Cells were then stained with $50 \mu\text{g mL}^{-1}$ DAPI for 30 min at room temperature. The cells undergoing apoptosis, represented by the morphological changes of apoptotic nuclei, were observed and imaged from ten eye views at 20x magnifications under a laser scanning confocal microscope LSM 710 (Zeiss).

Apoptosis evaluation - Flow cytometry

The MCF-7 cells were grown in a 6-well culture plate and exposed to IC_{50} concentrations of complex **1** for 24 h. The Annexin V-FITC kit uses annexin V conjugated with fluorescein isothiocyanate (FITC) to label phosphatidylserine sites on the membrane surface of apoptotic cells. Briefly the cells were trypsinised and washed with Annexin binding buffer and incubated with Annexin V FITC and PI for 30 min and immediately analysed using flow cytometer FACS Aria-II. The results were analysed using DIVA software and percentage positive cells were calculated.

Annexin V-Cy3 staining

Phosphatidylserine translocation from the inner to the outer leaflet of the plasma membrane is one of the early features of apoptosis. Cell surface phosphatidylserine was detected using phosphatidylserine-binding protein annexin V conjugated with Cy3 using the commercially available annexin V-Cy3 apoptosis detection kit (APOAC, Apoptosis Detection Kit, Sigma). MCF-7 cells were cultured and treated with the IC_{50} concentration of the complex **1** and incubated for 24 h. The cells were processed according to the instructions in the kit and observed in the fluorescent microscope. The combination of 6-carboxyfluorescein diacetate (6-CFDA) with annexin V conjugated to Cy3 in the kit allowed the differentiation of live cells (green), necrotic cells (red) and apoptotic cells (red and green). At random, 300 cells were observed, and the percentage of cells reflecting cell death (both apoptotic and necrotic) was calculated.

Reactive Oxygen Species (ROS) Assay.

For quantifying the intracellular ROS, 5×10^5 MCF-7 cells were seeded on a 6-well plate containing cover slip and incubated overnight for attachment. After incubation, the cells were treated with fresh medium containing lethal dose of complex **1** and incubated further for 24 h. At the end of incubation, cover slip was removed from the culture plate and stained with $40 \mu\text{M}$ of 2',7'-dichlorofluorescein-diacetate (DCFHDA) dye for 30 min. The stained cover slip was washed with PBS solution and visualized under fluorescence to record images.

Mitochondrial membrane potential Assay

Mitochondrial membrane potential, $\Delta\psi_m$ is an important parameter of mitochondrial function used as an indicator of

cell health. MCF-7 Cells treated overnight with complex **1** in 6-well plates were incubated for 1 h with $2 \mu\text{g mL}^{-1}$ of JC-1 in the culture medium. The adherent cell layer was then washed three times with PBS and dislodged with $250 \mu\text{L}$ of trypsin-EDTA. Cells were collected in PBS/2% bovine serum albumin (BSA), washed twice by centrifugation, resuspended in 0.3 mL of PBS/2% BSA, mixed gently, and examined in the fluorescent microscope (Carl Zeiss, Jena, Germany) using a UV filter (450–490 nm) at 400x magnifications.

Analysis of Mitochondrial Membrane Potential ($\Delta\psi_m$).

MCF-7 cells were treated with the IC_{50} concentrations of complex **1** for 24 h and collected by centrifugation. The cells were resuspended in pre-warmed JC-1 ($5 \mu\text{g/mL}$ in PBS) and incubated for 30 min at 37°C . Subsequently, the cells were washed twice with PBS, and were analyzed immediately using flow cytometer FACS Aria-II.

TUNEL assay

Apoptosis in MCF-7 cells was detected using TUNEL (terminal deoxynucleotidyl transferase dUTP nick-end labeling) apoptosis detection kit (Genscript, USA). MCF-7 and NIH 3T3 cells were cultured and treated with the IC_{50} concentration of the complex **1** and incubated for 24 h. Treated MCF-7 and NIH 3T3 cells were fixed with 4% paraformaldehyde and permeabilized with 0.1% Triton X-100. TUNEL DNA-end labeling was performed with biotinylated nucleotide-dUTP in the presence of terminal deoxynucleotidyl transferase. Then horseradish peroxidase-labeled streptavidin (Streptavidin-HRP) was bound to the biotinylated nucleotides, which were detected using the peroxidase substrate, hydrogen peroxide, and 3,3'-diaminobenzidine (DAB) solution. Using this procedure, apoptotic nuclei were stained dark brown and observed in a light microscope (Olympus, Japan).

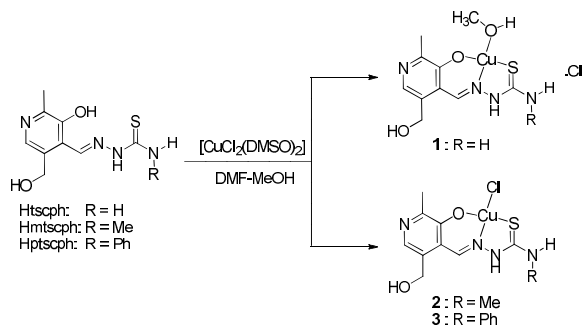
Results and discussion

Synthesis and characterization

Three new square planar copper(II) complexes containing substituted pyridoxal thiosemicarbazone ligands, have been obtained by the reaction of the $[\text{CuCl}_2(\text{DMSO})_2]$ with the corresponding Schiff bases (Scheme 1). All the copper(II) complexes $\{[\text{Cu}(\text{tscpy})(\text{MeOH})](\text{Cl})$ (**1**), $[\text{CuCl}(\text{mtscpy})]$ (**2**), $[\text{CuCl}(\text{ptscpy})]$ (**3**) $\}$, were characterized by elemental analysis, conductance, magnetic moment measurements as well as spectroscopic techniques (IR, UV-vis, EPR) and the significant data are given in the Experimental Section. The observed elemental (C, H, N) analysis data of **1-3** were in consistent with their composition and it appears from the formulation that the Schiff base coordinate to the copper(II) ion as monobasic tridentate ligand in all the three complexes. The IR peak shift in (C=N) and (C=S) and the absence of (O-H) of the coordinated ligands in the complexes gave evidence for the coordination of the ligand to copper(II) centre via phenolate-O, azomethine-N and thione-S.⁴¹ The magnetic moment values of **1-3** were in agreement of one unpaired electron and the observed g_{\parallel} and g_{\perp} values from EPR are similar to mononuclear Cu(II)

complexes.⁴² The molar conductance value for complex **1** was in the range for 1:1 electrolyte indicating that **1** has a cationic nature with one chloride anion located out of the coordination sphere as a counter ion whereas complexes **2** and **3** have non-electrolytic nature and are neutral complexes. The coordination mode of the thiosemicarbazone ligand and the overall coordination geometry of the complexes were further confirmed by X-ray single crystal structure analysis.

Scheme 1. Synthetic Route of the New Copper(II) Complexes



Crystal structure of the complexes 1 and 3

The ORTEP view of complex **1** along with the atomic numbering scheme is given in Figure 1 and the bond parameters involving the metal centre are given in Table S1 (ESI⁺). The crystallographic data showed that complex **1** is crystallized in a triclinic crystal system with the space group *P*₁. The Cu(II) ion adopts a distorted square-planar geometry with the binding of the ligand as monobasic tridentate (ONS donor) forming 5- and 6-membered fused chelate rings, and the fourth site is occupied by the oxygen atom of methanol molecule. The charge on the complex is neutralized by one chloride ion that is present in the lattice. Around the Cu(II) ion, the chelate bite angle in the five membered ring formed by the azomethine-N and thione-S atoms (86.70°) is slightly smaller than that in the six membered ring formed by the azomethine-N and the phenolate-O atoms (94.02°), indicating better chelation in the former ring. The trans angles of O(1)–Cu–S, 176.86(8)°, and N(1)–Cu–O(2), 172.81(12)°, indicated a slight deviation from the expected linear trans geometry due to the rigidity of the tridentate ligand and hence suggesting distortion in the square-planar coordination geometry. A small dihedral angle of 3.85° between the mean planes of the five member chelation ring and the six member one ensures that the planarity of square is appreciable. The analysis of the bond lengths and bond angles Table S1 (ESI⁺) further supports the belief that the ligand coordinates to the metal ion via the neutral thione sulphur.

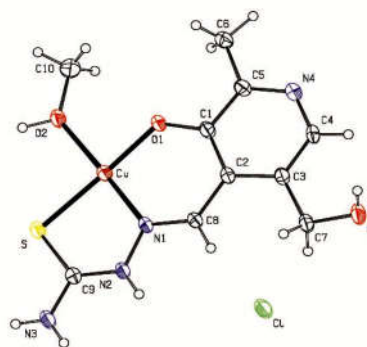


Figure 1. ORTEP view of complex **1** showing thermal ellipsoids at the 30% probability level

The ORTEP view of complex **3** together with the atomic numbering scheme is shown in Figure S1 (ESI⁺) whereas the selected bond lengths and bond angles are listed in Table S1 (ESI⁺). The single-crystal X-ray studies revealed that complex **3** crystallized in a monoclinic system with the space group *C2/c*. As seen in complex **1**, the coordination geometry around Cu(II) in complex **3** also is a distorted square-planar, the copper centre being bonded to uninegative tridentate ONS donor ligand molecules in such a way that a five- and a six-membered ring is formed. The chloride ion occupies the fourth coordination site. Therefore, Cu(II) centre is nested in a ONSCl core which is distorted from the ideal square planar geometry as manifested in the bond parameters around the metal center. As in the case of complex **1**, a smaller bite angle of the five-membered ring (85.68°) indicated better chelation than the six-membered chelate ring (91.80°). The trans angles are O(1)–Cu–S, 170.61(11)°, and N(1)–Cu–Cl, 171.62(12)°, showed a deviation from the expected linear trans geometry, suggesting distortion in the square-planar coordination geometry. The dihedral angle between the mean planes of the coordinating five-membered chelation ring and the six-membered one is 6.42°. The coordination of the ligand to the copper centre via the neutral thione sulphur was further validated from the analysis of the bond lengths and angles Table S1 (ESI⁺). The crystal structure also reveals the presence of two solvent (one DMF and one H₂O) molecules of crystallization.

Stability studies

Solubility is usually accepted as an important step for the function of Cu–DMSO compounds in biological systems. Thus, the solution chemistry of complexes **1–3** is analyzed by UV-visible spectroscopy. Compound **1** is highly soluble in water whereas, **2** and **3** is partially soluble in water. The complexes are first dissolved in DMSO, and the concentrated DMSO solutions were diluted using aqueous PBS buffer (phosphate buffered saline solution), at pH 7.4, to a final concentration of 1×10^{-3} M. The UV-visible absorption spectrum of these complexes is recorded for every 1 h over 24 h at room temperature. The spectral profiles for complexes **1–3** did not change which clearly indicate the stability of the nature of the

complexes in solution (Figure S2 (ESI[†])). The spectrum of the freshly prepared buffer solution of complexes **1-3** displayed two absorptions in the visible region at 330 nm and another less intense maximum located at 420 nm. Further ESI-MS of acetonitrile solution of complexes **1-3** exhibit base peaks at *m/z* 369.76, 352.83 and 413.72 respectively confirm the presence of monomeric entity in solution phase (Figure S3 (ESI[†])).⁴³

DNA binding studies

UV-Vis absorption titrations

Electronic absorption spectroscopy is one of the convenient tools for examining the binding characteristics between metal complexes and DNA. Therefore, before evaluating the potentials of antitumor activities of the complexes, the interaction between the DNA and the new synthesized complexes was examined by UV-visible absorption spectral titrations. The concentration of the complex was kept constant and DNA was added to that solution in increasing amounts. The binding of metal complex to DNA via intercalation is generally characterized by hypochromism along with or without a small shift in the wavelength in the absorption spectrum of the complex by virtue of the stacking interactions between the complex and the base pairs of DNA.⁴⁴ The extent of hypochromism and shift are commonly found to correlate with the intercalative binding strength. The absorption spectrum of representative complex **1** measured as a function of increasing concentration of CT-DNA is given in Figure 2 (complexes **2** and **3** S4 (ESI[†])). Upon incremental additions of DNA (0–50 μM) to the complexes **1-3**, significant changes were observed in the intensities ligand centered transitions and the charge-transfer transitions of the complexes ($\lambda_{\text{max}} \sim 329$ nm and ~ 415 nm) which were found to decrease with a small red shift of about 2 nm suggesting intercalative mode of binding of the complexes to DNA.⁴⁵ After the complexes intercalate to the base pairs of DNA, the π^* orbital of the intercalated complexes could couple with π orbitals of the base pairs, decreasing the π - π^* transition energies and resulting in hypochromism. The absorption bands of the cationic complex **1** at 329 nm and 415 nm exhibited greater hypochromism ($\sim 54\%$, $\sim 61\%$) when compared to the neutral complexes **2** ($\sim 48\%$, $\sim 49\%$) and **3** ($\sim 52\%$, $\sim 57\%$), indicating that the binding strength of complex **1** is much stronger than that of the other two complexes.

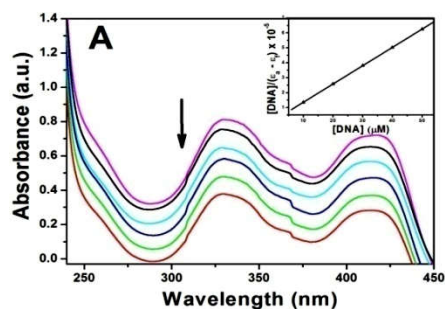


Figure 2. Electronic spectra of complexes **1** (A) in Tris-HCl buffer upon addition of CT-DNA. [Complex] = 25 μM, [DNA] =

0–50 μM. Arrow shows the absorption intensities decrease upon increasing DNA concentration. (Inset) Plots of $[DNA]/(\epsilon_a - \epsilon_f)$ versus $[DNA]$ for complex **1** with CT-DNA.

In order to compare quantitatively the binding strength of the complexes, the intrinsic binding constants (K_b) were determined from the following equation: $[DNA]/(\epsilon_a - \epsilon_f) = [DNA]/(\epsilon_b - \epsilon_f) + 1/K_b(\epsilon_b - \epsilon_f)$, where $[DNA]$ is the concentration of DNA in the base pairs, ϵ_a is the apparent absorption coefficient corresponding to $A_{\text{obs}}/[\text{complex}]$, ϵ_f is the extinction coefficient of the complex free in solution and ϵ_b is the extinction coefficient of the complex when fully bound to DNA.⁴⁶ A plot of $[DNA]/(\epsilon_a - \epsilon_f)$ versus $[DNA]$ (inset, Figure 3) gave a slope and a y-intercept of $1/(\epsilon_b - \epsilon_f)$ and $1/K_b(\epsilon_b - \epsilon_f)$ respectively. The intrinsic binding constant (K_b) is ratio of the slope to the intercept. The K_b values were found to be $1.15 (\pm 0.02) \times 10^5 \text{ M}^{-1}$, $0.52 (\pm 0.06) \times 10^5 \text{ M}^{-1}$ and $0.82 (\pm 0.04) \times 10^5 \text{ M}^{-1}$ for **1-3** respectively. The obtained magnitude of K_b clearly indicated that the complexes **1-3** bind to DNA via the intercalative mode. The observed binding constants revealed that the cationic complex **1** has higher magnitude of binding than the neutral complexes **2** and **3** with CT-DNA and the order of binding affinity is **2** < **3** < **1**. From the K_b values obtained, it can be inferred that the cationic nature, enhanced water solubility and preferring interaction of the complex **1** with the DNA bases through π - π^* interaction increases the binding ability with CT-DNA when compared to the neutral complexes **2** and **3**. The complex **3** strongly binds with CT-DNA when compared to the complex **2**, which may be due to the presence of the phenyl ring in the terminal nitrogen of the respective ligand, preferring interaction of the complex with the DNA bases through π - π^* interaction. Though it has been found that complexes **1-3** can bind to DNA by intercalation, the binding mode needs to be proved through further experiments.

Ethidium bromide displacement studies

The absorption titration results indicate that the complexes effectively bind to DNA. All the three complexes **1-3** were non-emissive and in order to confirm the binding mode and compare their binding affinities, competitive binding studies using ethidium bromide (EB) bound to DNA were carried out for the complexes. EB is a planar, cationic dye, and is one of the most sensitive fluorescence probes for DNA. EB emits intense fluorescent light in the presence of DNA due to its strong intercalation between the adjacent DNA base pairs.⁴⁷ The quenching of emission intensity of EB bound to DNA occurs as the planar rings in complexes can efficiently compete with EB for intercalative binding sites on DNA by replacing EB.

The emission quenching spectra of the EB bound to DNA by the complex **1** is shown in the Figure S5 (ESI[†]). As the concentration of the complexes increases (0 – 25 μM), the emission band at 599 nm exhibited hypochromism up to 21, 19 and 20% of the initial fluorescence intensity for **1**, **2** and **3** respectively. The observed decrease in the fluorescence intensity clearly indicates that the EB molecules are displaced from their DNA binding sites and are replaced by the

complexes under investigation.⁴⁸ In addition, the quenching data were analyzed according to the linear Stern-Volmer equation, $I_0/I = K_q[Q] + 1$, where, I_0 is the emission intensity in the absence of the complex (quencher), I is the emission intensity in the presence of the quencher, K_q is the linear Stern-Volmer quenching constant, and $[Q]$ is the concentration of the quencher. The K_q value is obtained as a slope from the plot of I_0/I versus $[Q]$. From the Stern-Volmer plot (inset, Figure 4) of I_0/I versus $[Q]$, the quenching constant (K_q) values were obtained from the slope. The K_q values were found to be $1.02 (\pm 0.13) \times 10^5 \text{ M}^{-1}$, $1.18 (\pm 0.10) \times 10^5 \text{ M}^{-1}$ and $1.10 (\pm 0.19) \times 10^5 \text{ M}^{-1}$ for **1**, **2** and **3** respectively.

Further, the apparent DNA binding constant (K_{app}) values were also calculated using the equation: $K_{EB} \times [EB] = K_{app} \times [\text{complex}]_{50}$, where, $[\text{complex}]_{50}$ is the concentration of the complex at 50% quenching of the emission intensity of EB bound to DNA, K_{EB} ($1.0 \times 10^7 \text{ M}^{-1}$) is the DNA binding constant of EB, $[EB]$ is the concentration of EB (12 μM). The calculated K_{app} values were $4(\pm 0.18) \times 10^5 \text{ M}^{-1}$, $5.03 (\pm 0.12) \times 10^5 \text{ M}^{-1}$ and $4.67 (\pm 0.17) \times 10^5 \text{ M}^{-1}$ for **1**, **2** and **3** respectively. The trend in K_{app} values are in line with the trend in the K_b values which were obtained from the UV-Vis absorption spectral studies. The higher K_q and K_{app} values of **1** than **2** and **3** may be attributed to its cationic nature and higher solubility in aqueous medium. The quenching and binding constants of the copper(II) complexes suggested that the interaction of complexes **1-3** with DNA should be of intercalation.⁴⁹

Circular dichroic spectral studies

The CD spectral analysis gives valuable evidence on the binding mode of metal complexes with DNA. The B form of DNA exhibited two conserved bands in the UV-region, a positive band at 278 nm due to base stacking interaction and a negative peak at 247 nm due to right handed helicity which are very sensitive to the mode of the DNA interaction with small molecules. Simple groove binding and electrostatic interaction of molecules exhibits a small or no perturbation on the base stacking and helicity of DNA, whereas intercalation enhances the intensities of both the bands stabilizing the right-handed B form of DNA as observed for the classical intercalators.⁵⁰ These conformational changes are in the order of $2 < 3 < 1$ which indicate that cationic and neutral complexes **1-3** plays a major role for the conformational changes of DNA due to groove binding/partial intercalation (Figure S6).

Viscosity studies

To further confirm the nature of interaction between the copper(II) complexes **1-3** and DNA, viscosity measurements were carried out for DNA in the absence and presence of complexes. In general, intercalative ligands are expected to elongate the DNA double helix by accommodating the ligands in between the base pairs, leading to an increase in the viscosity of DNA. In contrast, a partial, non-classical intercalation of ligand could bend (or kink) DNA helix, reducing its length and thereby its viscosity (Figure S7). Plot of the relative specific viscosity $(\eta/\eta_0)^{1/3}$ to $[\text{complex}]/\text{DNA}$

shows that upon increasing the concentration of the copper(II) complexes, a relatively insignificant decrease in DNA viscosity was observed. Based on these changes in DNA viscosity it is clear that copper(II) complexes interact with CT-DNA by groove binding or partial intercalation.⁵¹ The ability of the complexes to increase the viscosity of DNA follows the order $2 < 3 < 1$.

Cleavage of pUC19 DNA by Copper(II) complexes

In order to ascertain the DNA cleavage ability of complexes **1-3** supercoiled (SC) pUC19 DNA incubated with increasing concentration of complex in 5 mM Tris-HCl/40 mM NaCl buffer solution (pH 7.2) for 45 min without addition of any reductant. The activity of complexes **1-3** was assessed by the conversion of pUC19 DNA from Form I (supercoiled form) to Form II (nicked circular). The concentration dependent DNA cleavage activity of complexes **1-3** was observed by gel electrophoresis (Figure S8). With increase in concentration of complexes **1-3**, the amount of Form I of pUC19 DNA gradually diminishes whereas Form II increases, suggesting the single strand DNA cleavage. At 25 μM concentration, complexes exhibited efficient nuclease activity, the supercoiled form (Form I) relaxes to generate nicked form (Form II). However, in the case of complex **1** there was a complete conversion of Form I into Form II which reveals a higher cleavage efficiency of complex **1** in compare to complex **2-3**; with an increase in concentration, an intensified nicked form (Form II) was observed. From the cleavage patterns it was clearly observed that the intensity of Form II of DNA was higher in complex **1** than complex **2-3**, which corroborated well with the DNA binding studies.⁵² The DNA cleavage activity carried out with complex **1** are not inhibited by the presence of various radical scavengers, that is, NaN_3 , superoxide dismutase, DMSO and ethanol (Figure S9).

T4 DNA ligase assay

DNA religation experiment was performed to confirm the DNA cleavage by hydrolytic pathway in the presence of complexes **1-3**. The supercoiled (SC) pUC19 DNA was treated with a T4 DNA ligase enzyme and subjected to gel electrophoresis. The complexes **1-3** yielded linearized DNA which was religated using T4 DNA ligase enzyme. It has been observed that DNA cleavage by complex **1** is not inhibited by the presence of hydroxyl radical scavenger (H_2O_2). The experimental results show that the nicked form (Form II) was religated to a large extent in comparison to control DNA in the supercoiled form (Figure S10), providing a strong evidence in favour of hydrolytic pathway.⁵³

Protein binding studies

An analysis of the binding of chemical compounds to BSA is commonly investigated by examining fluorescence spectra. The interaction of BSA with the copper(II) complexes **1-3** was studied by fluorescence measurement at room temperature. A solution of BSA (1 μM) was titrated with various

concentrations of the complexes **1-3** (0 – 25 μM) and the fluorescence spectra were recorded in the range of 300–400 nm upon excitation at 280 nm. The effects of the complexes on the fluorescence emission spectrum of BSA is given in Figure S11 (ESI⁺). For each copper(II) complex, it was found that the emission of BSA at 349 nm was increasingly quenched when titrated with increasing concentration of the copper(II) complex. A significant decrease of the fluorescence intensity of BSA up to 61.81, 55.20 and 58.23%, from the initial fluorescence intensity of BSA, accompanied by a hypsochromic shift of 1–3 nm was observed for complexes **1-3** respectively revealing a definite interaction of all the three complexes with the BSA protein.⁵⁴ To have a deep insight into the quenching progression, the quenching constant (K_q) was evaluated following Stern–Volmer equation. From the plot of I_0/I versus $[Q]$ Figure S12 (ESI⁺), K_q can be calculated (Table 2).

Table 2: Quenching constant (K_q), binding constant (K_{bin}) and number of binding sites (n) for the interaction of complexes with BSA.

Complexes	K_q (M ⁻¹)	K_{bin} (M ⁻¹)	n
1	$1.08 (\pm 0.03) \times 10^6$	$2.03 (\pm 0.05) \times 10^5$	1.18
2	$1.07 (\pm 0.07) \times 10^5$	$4.15 (\pm 0.03) \times 10^4$	1.06
3	$1.21 (\pm 0.04) \times 10^5$	$8.90 (\pm 0.05) \times 10^4$	1.10

If it is assumed that the binding of complexes with BSA occurs at equilibrium, the equilibrium binding constant can be analyzed according to the Scatchard equation, $\log[(I_0 - I)/I] = \log K_{\text{bin}} + n \log[Q]$, where K_{bin} is the binding constant of the complex with BSA and n is the number of binding sites. K_{bin} and n have been calculated from the plot of $\log[(I_0 - I)/I]$ versus $\log[Q]$ Figure S12 (ESI⁺) and Table 2. For all the complexes, the estimated value of n (~ 1) strongly supported the existence of a single binding site in BSA⁵⁵ for **1-3**. However, the values of K_q and K_{bin} showed that among the three Cu(II) complexes, the cationic complex **1** has better interaction with BSA relative to other two neutral complexes under investigation.

In vitro cytotoxic assay

Encouraged by the positive results obtained from the previous biological studies, namely, DNA binding / cleavage and BSA binding for the copper complexes **1-3**, the cytotoxic activity of these complexes were tested against a panel of cell lines such as HeLa, MCF-7 and Hep G2 and cell viability was determined using MTT assay. The IC_{50} values of the complexes **1-3** are listed in Table 3. As shown in (Figure S13 (ESI⁺)), the complexes showed the viability of the HeLa, MCF-7 and HepG2 cells in a dose-dependent manner. From the IC_{50} values obtained it was inferred that the Cu(II) complexes **1-3** were active against HeLa, MCF-7 and Hep G2 cell lines and they possess great selectivity towards MCF-7 than HeLa and Hep G2 cell lines indicating that the complexes were more specific on a particular cancer cell (MCF-7). The activity of complex **1** was significantly superior than that of the well-known anticancer drug cisplatin, whereas the activity of complexes **2**

and **3** was significantly inferior than that of cisplatin. In addition, the *in vitro* cytotoxic activity studies of the new complexes against the mouse embryonic fibroblast cell line NIH 3T3 (normal cells) was undertaken and the IC_{50} value of the complexes have been found to be above 135 μM , which confirmed that the complexes are very specific on cancer cells. The IC_{50} values of the copper(II) complexes (including K_b value) have been compared with other recently reported copper complexes.⁵⁶

Table 3. IC_{50} values (μM) of cancer cell lines

Complexes	IC_{50} values (μM)			
	HeLa	MCF-7	Hep G2	NIH3T3
Complex 1	15.06 (± 1.0)	3.36 (± 0.6)	12.3 (± 1.2)	149.21 (± 1.2)
Complex 2	28.07 (± 1.9)	16.01 (± 1.1)	28.1 (± 2.1)	135.46 (± 0.6)
Complex 3	23.04 (± 1.4)	14.01 (± 0.8)	23.7 (± 1.9)	143.92 (± 2.4)
Cisplatin	19.3 (± 1.2)	12.4 (± 0.5)	24.1 (± 1.2)	141.35 (± 1.5)

Morphological changes in AO and EB dual staining

An Acridine Orange–Ethidium Bromide and (AO–EB) dual staining experiment was performed in MCF-7 cells with the copper complex **1** to further investigate its ability to induce cell death. The experiment was based on the discrimination of live cells from the dead cells on the basis of morphological changes. AO, which can pass through the plasma membrane, stains the DNA of live cells and fluoresces green. EB on the other hand is excluded from the cells having intact plasma membrane and stains the DNA of dead cells, showing orange fluorescence. The cells were incubated with the complex **1** for 2 h and irradiated with visible light showed significant reddish–orange emission characteristic of the apoptotic cells. The controls, which were incubated in dark, showed only predominant green emission (Figure 3). Hence, the observed morphological changes reveal that the complex **1** induces cell death only through apoptosis and not through necrosis.⁵⁷

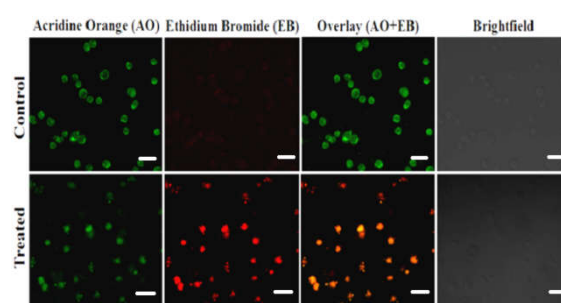


Figure 3. Morphological assessment of AO and EB dual staining of MCF-7 cells treated with complex **1** (IC_{50} concentration) for 24 h. The scale bar 20 μm .

Nuclear DAPI staining

To further confirm the apoptosis mode, DAPI staining was also carried out. The control and complex **1** treated cells were stained with DAPI and observed under confocal microscope

(Figure 4). The control cells permeabilized with detergent (0.1% Triton X-100) exhibit light and evenly stained contours of the nuclei in contrast to the treated cells that show typical characteristics of cells undergoing apoptosis. The treated cells are seen to possess fragmented or highly condensed nuclei while the bright field images provide evidence for cell shrinkage and membrane blebbing attributed to the typical features of apoptotic cells. Thus the DAPI staining indicates apoptotic mode of cell death with the complex **1**.⁵⁸

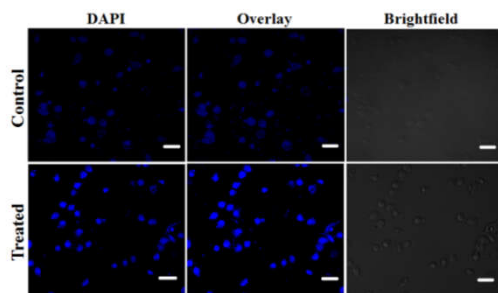


Figure 4. Morphological assessment of complex **1** (IC_{50} concentration) and MCF-7 cells for 24 h. The scale bar 20 μm .

Evaluation of Apoptosis - Flow Cytometry

The ability to induce apoptosis by copper(II) complex was further determined with the help of flow cytometry, using the Annexin V-FITC Apoptosis Detection Kit to perform double-staining with propidium iodide and Annexin V-FITC. Annexin V, a Ca^{2+} dependent phospholipid-binding protein with a high affinity for the membrane phospholipid phosphatidylserine (PS), is quite helpful for identifying apoptotic cells with exposed PS. Propidium iodide is a standard flow cytometric viability probe used to distinguish viable from non-viable cells (Figure 5). The MCF-7 cells were treated with the complex **1** at IC_{50} concentrations for 24 h. Annexin V⁺/PI⁺ (Q2) population represented cells undergoing apoptosis of 56.2% for IC_{50} concentrations of the complex **1**.⁵⁹

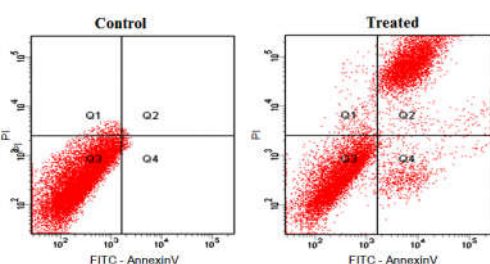


Figure 5. AnnexinV/propidium iodide assay of MCF-7 cells treated by complex **1** (IC_{50} concentration) measured by flow cytometry.

Annexin V-FITC staining assay

The characteristic morphological changes brought about in the cells by treatment with Complex **1** have been evaluated by adopting fluorescent microscopic analysis Annexin V-FITC stained cells. The control viable cells have uniformly green fluorescing nuclei and a highly organized structure. After cells

were treated with IC_{50} concentration of the complex **1** for 24 h, we have observed cytological changes like late apoptotic cells that have red fluorescing nuclei (Figure S14) with condensed or fragmented chromatin and necrotic cells, swollen to large sizes that have uniformly red fluorescing nuclei with no indication of chromatin fragmentation by staining. The results indicate that the complex **1** induce cell death through apoptosis or necrosis.⁶⁰

Reactive oxygen species (ROS) detection

The intracellular – reactive oxygen species are chemically important reactive molecules containing oxygen that regulates normal cellular process. However, dysregulation of ROS generation dramatically affects cell structure and may result in cellular damage leading to a wide range of human diseases. Hence, in the present study ROS levels in MCF-7 cancer cell line are probed by using an oxidant sensitive fluorescent dye. Dichloro-dihydro-fluorescein diacetate (DCFH-DA) is a non-polar cell-permeable fluorescent dye that can be converted into polar DCFH by cellular esterase. However, this DCFH is undetectable under microscope and requires intracellular ROS to switch them into a highly fluorescence emitting DCF. Our result indicates that complex **1** treated with MCF-7 cells is shown to fluorescence rather than no fluorescence which was observed in control cells (Figure S15). This infers complex **1** stimulate ROS induced apoptosis in MCF-7 cells.⁶¹

Mitochondrial membrane potential detection

Mitochondrial dysfunction is involved in apoptotic cell death. Mitochondria play important roles in apoptosis through the release of proapoptotic factors such as cytochrome *c* and other apoptosis-inducing factors. Cationic JC-1 was used as a fluorescence probe in detecting the changes of mitochondrial membrane potential ($\Delta\Psi_m$) induced by complex **1**. JC-1 exhibits potential-dependent accumulation in mitochondria, indicated by a fluorescence emission shift from red (~ 590 nm) to green (~ 525 nm). This study confirms the cell apoptosis induced by complex **1** the changes in the mitochondrial membrane potential in MCF-7 cells (Figure 6). The mitochondrial membrane potential level was decreased on increasing time of complex **1** IC_{50} concentration with MCF-7 cells.⁶² The change of $\Delta\Psi_m$ was further confirmed by flow cytometry analysis of complex **1** treated MCF-7 cells using JC-1 dye. The mitochondrial stain JC-1 can spontaneously aggregate as J-aggregates, which will emit red fluorescence at high membrane potential in healthy cells, whereas in the apoptotic cells, JC-1 would remain green fluorescent monomers due to mitochondrial membrane depolarization. The change of $\Delta\Psi_m$ in MCF-7 cells induced by complex **1** is shown in Figure 7. This indicates that the induction of apoptosis by complex **1** is associated with the mitochondrial (intrinsic) pathway.⁶³

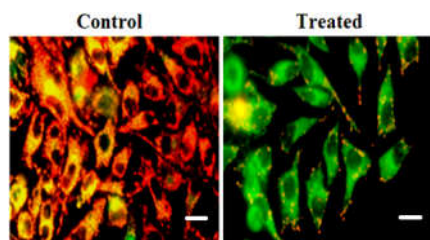


Figure 6. MCF-7 cells were treated with complex **1** (IC_{50} concentration) for 24 h. The scale bar 40 μ m.

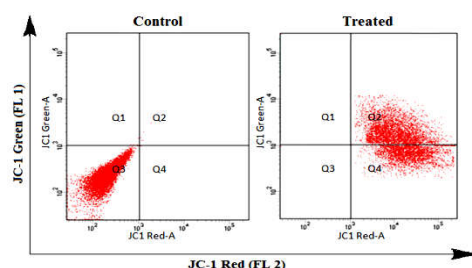


Figure 7. Flow cytometric analysis (FACS) of the mitochondrial membrane potential using the JC-1 dye in MCF-7 cells were treated with complex **1** (IC_{50} concentration) for 24 h.

TUNEL assay

TUNEL assay was performed to confirm complex **1** treatment induced apoptosis. TUNEL is one of the most popular methods for identifying apoptotic cells in situ by detecting DNA fragmentation. Due to activation of Ca/Mg dependent endonucleases in apoptotic cells, DNA is cleaved. These DNA strand breaks of cleaved can be identified by deoxynucleotidyl transferase that catalyzed the addition of biotin-dUTP. The control cells show normal nuclear morphology. MCF-7 (cancer cell) Cells (Figure 8) and NIH 3T3 (normal cell) cells (Figure S16) treated with complex **1** (IC_{50} concentration) for 24 h are notably TUNEL-positive and show apoptotic bodies and fragmented or condensed nuclei. The biotin-labeled cleavage sites are then detected by reaction with streptavidin-HRP and the brown color is visualized by DAB.⁶⁴

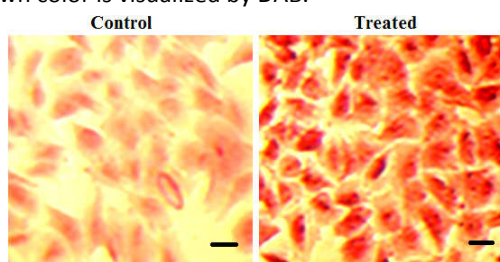


Figure 8. TUNEL assay of MCF-7 cells were treated with complex **1** for 24 h. The scale bar 20 μ m.

Conclusion

A series of water soluble square-planar copper(II) complexes (**1-3**) containing substituted pyridoxal thiosemicarbazone

ligands were synthesized and characterized adequately by analytical and spectral techniques. The single crystal X-ray diffraction study of the cationic complex **1** and the neutral complex **3** revealed that the ligand coordinated to the Cu(II) centre via phenolic-O, azomethine-N and thione-S in a monoanionic tridentate fashion. The CT-DNA binding experiments showed that all the complexes bind with DNA via partial intercalation or groove binding. The gel electrophoresis assay demonstrated that all the complexes have been found to promote the cleavage ability of the supercoiled pUC19 DNA to the nicked circular form in the absence of any external agents. Elucidation of the mechanistic pathway by T4 ligase experiment suggested that all the complexes cleave DNA through a hydrolytic pathway. In addition, the protein binding properties of the new complexes were studied using fluorescence spectroscopic techniques. Further, all the new complexes were screened for cytotoxic activity against HeLa, MCF-7 and Hep G2 cancer cell lines, and they were found to exhibit excellent cytotoxicity to cancer cell without affecting the normal NIH 3T3 cells. The activity of complex **1** was significantly superior to that of cisplatin. Complex **1** was shown to accumulate preferentially in the MCF-7 cells and induced apoptosis which involved ROS generation, mitochondrial membrane potential, Annexin V-FITC assay, TUNEL assay and FACS analysis. Thus, the complex **1** shows effective antiproliferative effects and has the potential to be developed as a chemotherapeutic agent for the treatment of various cancer diseases.

Acknowledgements

One of the authors (MMS) thank the University Grants Commission (UGC), New Delhi for financial assistance through the UGC-BSR for financial support (Junior Research Fellowship) BSR fellowship (Ref. No. F.7-22/2007(BSR)). The EPR and fluorescence spectral facilities in the School of Chemistry, Bharathidasan University, funded by the UGC-SAP, New Delhi, are gratefully acknowledged. Dr. Sanjeev Kanojiya, CDRI- Lucknow, for providing the ESI-MS facilities. The use of the single-crystal diffractometer facility at the School of Chemistry, University of Hyderabad, is gratefully acknowledged. We thank Dr. T. R. Santhosh Kumar for the flow cytometry analysis.

REFERENCES

- 1 X. Wang, Z. Guo, *Chem. Rev.*, 2013, **42**, 202-224.
- 2 E. Gabano, M. Ravera, D. Osella, *Dalton Trans.*, 2014, **43**, 9813-9820.
- 3 E.R. Jamieson, S.J. Lippard, *Chem. Rev.*, 1999, **99**, 2467-2498.
- 4 C.A. Rabik, M.E. Dolan, *Cancer Treat. Rev.*, 2007, **33**, 9-23.
- 5 N.J. Wheate, S. Walker, G.E. Craig, R. Oun, *Dalton Trans.*, 2010, **39**, 8113-8127.
- 6 J. Reedijk, *Eur. J. Inorg. Chem.*, 2009, 1303-1312.
- 7 W. Han Ang, P. J. Dyson, *Eur. J. Med. Chem.*, 2006, 4003-4018.
- 8 J. Lakshmi Praba, S. Arunachalam, A. Riyasdeen, R. Dhivya, M.A. Akbarsha, *J. Photochem. Photobiol. B*, 2015, **142**, 59-67.

- 9 G. Gasser, I. Ott, N. Metzler-Nolte, *J. Med. Chem.*, 2011, **54**, 3–25.
- 10 A. Gautier, F. Cisnetti, *Metallomics*, 2012, **4**, 23–32.
- 11 P.S. Donnelly, J.R. Liddell, S. Lim, B.M. Paterson, M.A. Cater, M.S. Savva, A.I. Mot, J.L. James, I.A. Trounce, A.R. White, P.J. Crouch, *Proc. Natl. Acad. Sci. U.S.A.* 2012, **109**, 47–52.
- 12 C. Santini, M. Pellei, V. Gandin, M. Porchia, F. Tisato, C. Marzano, *Chem. Rev.*, 2014, **114**, 815–862.
- 13 L. Tripathi, P. Kumar, A.K. Singhai, *Indian J. Cancer*, 2007, **44**, 62–71.
- 14 S. Dhar, D. Senapati, P.K. Das, P. Chattopadhyay, M. Nethaji and A.R. Chakravarty, *J. Am. Chem. Soc.*, 2003, **125**, 12118–12124.
- 15 C.H. Ng, K.C. Kong, S.T. Von, P. Balraj, P. Jensen, E. Thirthagiri, H. Hamada, M. Chikira, *Dalton Trans.*, 2008, 447–454.
- 16 A. Barve, A. Kumbhar, M. Bhat, B. Joshi, R. Butcher, U. Sonawane, R. Joshi, *Inorg. Chem.*, 2009, **48**, 9120–9132.
- 17 J. Lakshmi Praba, S. Arunachalam, D.A. Gandhi, T. Thirunalasundari, *Eur. J. Med. Chem.*, 2011, **46**, 3013–3021.
- 18 J.D. Ranford, P.J. Sadler, D.A. Tocher, *Dalton Trans.*, 1993, 3393–3399.
- 19 E. Sundaravadivel, S. Vedavalli, M. Kandaswamy, B. Varghese, P. Madankumar, *RSC Adv.*, 2014, **4**, 40763–40775.
- 20 J. Luis García-Giménez, M. González-Álvarez, M. Liu-González, B. Macías, J. Borrás, G. Alzuet, *J. Inorg. Biochem.*, 2009, **103**, 923–934.
- 21 B. P. Espósito, Najjar, *Coord. Chem. Rev.*, 2002, **232**, 137–149.
- 22 Z. Zhang, L. Jin, X. Qian, M. Wei, Y. Wang, J. Wang, Y. Yang, Q. Xu, Y. Xu, F. Liu, *ChemBioChem.*, 2007, **8**, 113–121.
- 23 I. Kostova, *Recent Pat. Anti-Cancer Drug Discovery*, 2006, 1–22.
- 24 (a) C. Marzano, M. Pellei, F. Tisato, C. Santini, *Anti-Cancer Agents Med. Chem.*, 2009, **9**, 185–211. (b) M. Belicchi-Ferrari, F. Bisceglie, C. Casoli, S. Durot, I. Morgenstern-Badarau, G. Pelosi, E. Pilotti, S. Pinelli and P. Tarasconi, *J. Med. Chem.*, 2005, **48**, 1671–1675. (c) M. B. Ferrari, F. Bisceglie, G. Pelosi, P. Tarasconi, R. Albertini, P. P. Dall'Aglio, S. Pinelli, A. Bergamo and G. Sava, *J. Inorg. Biochem.*, 2004, **98**, 301–312.
- 25 R.W. Brockman, J.R. Thomson, M.J. Bell, H.E. Skipper, *Cancer Res.*, 1956, **16**, 167–170.
- 26 D. Palanimuthu, S.V. Shinde, K. Somasundaram, A.G. Samuelson, *J. Med. Chem.*, 2013, **56**, 722–734.
- 27 P.J. Jansson, P.C. Sharpe, P.V. Bernhardt, D.R. Richardson, *J. Med. Chem.*, 2010, **53**, 5759–5769.
- 28 Saswati, A. Chakraborty, S.P. Dash, A.K. Panda, R. Acharyya, A. Biswas, S. Mukhopadhyay, S.K. Bhutia, A. Crochet, Y.P. Patil, M. Nethaji, R. Dinda, *Dalton Trans.*, 2015, **44**, 6140–6157.
- 29 S. Lim, K.A. Price, S.F. Chong, B.M. Paterson, A. Caragounis, K.J. Barnham, P.J. Crouch, J. M. Peach, J.R. Dilworth, A.R. White, P.S. Donnelly, *J. Biol. Inorg. Chem.*, 2010, **15**, 225–235.
- 30 W.L.F. Armarego, C.L.L. Chai, *Purification of Laboratory Chemicals*, sixth ed. Butterworth-Heinemann, Oxford, UK, 2009, pp. 69–79.
- 31 Z. Szafran, R. Pike, M. Singh, *Microscale Inorganic Chemistry*, John Wiley & Sons: New York, 1991, pp. 218–222.
- 32 E.W. Yemeli Tido, E.J.M. Vertelman, A. Meetsma, P. J. van Koningsbruggen, *Inorg. Chim. Acta*, 2007, **360**, 3896–3902.
- 33 SMART Version 5.630 and SAINT-plus Version 6.45 (2003) Bruker-Nonius Analytical X-ray Systems Inc., Madison, Wisconsin, USA.
- 34 G. M. Sheldrick, (1997) SADABS, *Program for Area Detector Absorption Correction*, University of Göttingen, Göttingen, Germany
- 35 G.M. Sheldrick, *Acta Crystallogr.*, 2008, **A64**, 112–122.
- 36 L.J. Farrugia, *J. Appl. Crystallogr.*, 1999, **32**, 837–838.
- 37 A.L. Spek, (2002) *Platon, A Multipurpose Crystallographic Tool*, Utrecht University, Utrecht, The Netherlands
- 38 C.F. Macrae, I.J. Bruno, J.A. Chisholm, P.R. Edgington, P. McCabe, E. Pidcock, L. Rodriguez-Monge, R. Taylor, J. van de Streek, P.A. Wood, *J. Appl. Cryst.*, 2008, **41**, 466–470.
- 39 A. Tarushi, E. Polatoglou, J. Kljun, I. Turel, G. Psomas, D. P. Kessissoglou, *Dalton Trans.*, 2011, 40, 9461–9473.
- 40 S. Ramakrishnan, D. Shakthipriya, E. Suresh, V. S. Periasamy, M. A. Akbarsha and M. Palaniandavar, *Inorg. Chem.*, 2011, **50**, 6458–6471.
- 41 S. A. Ingle, A. N. Kate, A. A. Kumbhar, A. A. Khan, S. S. Rao and S. P. Gejji, *RSC Adv.* 2015, **5**, 47476–47487.
- 42 M. Chauhan, K. Banerjee and F. Arjmand, *Inorg. Chem.*, 2007, **46**, 3072–3082.
- 43 Q.-P. Qin, Y.-C. Liu, H.-L. Wang, J.-L. Qin, F.-J. Cheng, S.-F. Tang and H. Liang, *Metallomics*, 2015, **7**, 1124–1136.
- 44 D. Senthil Raja, N.S.P. Bhuvanesh, K. Natarajan, *Eur. J. Med. Chem.*, 2012, **47**, 73–85.
- 45 M. Baldini, M. Belicchi-Ferrari, F. Bisceglie, P. P. Dall'Aglio, G. Pelosi, S. Pinelli and P. Tarasconi, *Inorg. Chem.*, 2004, **43**, 7170–7179.
- 46 A. Wolfe, G.H. Shimer, T. Meehan, *Biochemistry*, 1987, **26**, 6392–6396.
- 47 F.J. Meyer-Almes, D. Porschke, *Biochemistry*, 1993, **32**, 4246–4253.
- 48 L. Changzheng, W. Jigui, W. Liufang, R. Min, J. Naiyong, G. Jie, *Inorg. Biochem.*, 1999, **73**, 195–202.
- 49 Z.C. Liu, B.D. Wang, Z.Y. Yang, Y. Li, D.D. Qin, T.R. Li, *Eur. J. Med. Chem.*, 2009, **44**, 4477–4484.
- 50 Saswati, A. Chakraborty, S. P. Dash, A. K. Panda, R. Acharyya, A. Biswas, S. Mukhopadhyay, S. K. Bhutia, A. Crochet, Y. P. Patil, M. Nethaji and R. Dinda, *Dalton Trans.*, 2015, **44**, 6140–6157.
- 51 P. Gurumoorthy, D. Mahendiran, D. Prabhu, C. Arulvasu and A. K. Rahiman, *J. Mol. Struct.*, 2015, **1080**, 88–98.
- 52 (a) S. Banerjee, S. Mondal, S. Sen, S. Das, D. L. Hughes, C. Rizzoli, C. Desplanches, C. Mandal and S. Mitra, *Dalton Trans.*, 2009, 6849–6860; (b) S. Tabassum, M. Zaki, M. Afzal and F. Arjmand, *Dalton Trans.*, 2013, **42**, 10029–10041.
- 53 C. Sissi, F. Mancin, M. Gatos, M. Palumbo, P. Tecilla and U. Tonellato, *Inorg. Chem.*, 2005, **44**, 2310–2317.
- 54 N. Shahabadi and M. Maghsudi, *J. Mol. Struct.*, 2009, **929**, 193–199.
- 55 A. D. Tinoco, E. V. Eames, C. D. Incarvito and A. M. Valentine, *Inorg. Chem.*, 2008, **47**, 8380–8390.
- 56 V. Gandin, F. Tisato, A. Dolmella, M. Pellei, C. Santini, M. Giorgetti, C. Marzano and M. Porchia, *J. Med. Chem.*, 2014, **57**, 4745–4760.
- 57 U. Basu, I. Khan, A. Hussain, B. Gole, P. Kondaiah and A. R. Chakravarty, *Inorg. Chem.*, 2014, **53**, 2152–2162.
- 58 J. P. Johnpeter, G. Gupta, J. M. Kumar, G. Srinivas, N. Nagesh and B. Therrien, *Inorg. Chem.*, 2013, **52**, 13663–13673.
- 59 K.-B. Huang, Z.-F. Chen, Y.-C. Liu, X.-L. Xie and H. Liang, *RSC Adv.*, 2015, **5**, 81313–81323.
- 60 S. Anbu, M. Kandaswamy, S. Kamalraj, J. Muthumarry and B. Varghese, *Dalton Trans.*, 2011, **40**, 7310–7318.
- 61 C. Qian, J.-Q. Wang, C.-L. Song, L.-L. Wang, L.-N. Ji and H. Chao, *Metallomics*, 2013, **5**, 844–854.
- 62 J. Xu, F. Zeng, H. Wu and S. Wu, *J. Mater. Chem. B*, 2015, **3**, 4904–4912.
- 63 K. Du, J. Liang, Y. Wang, J. Kou, C. Qian, L. Ji and H. Chao, *Dalton Trans.*, 2014, **43**, 17303–17316.
- 64 S. Liu, W. Cao, L. Yu, W. Zheng, L. Li, C. Fan and T. Chen, *Dalton Trans.*, 2013, **42**, 5932–5940.

